Bioelectromagnetics 33:55–64 (2012)

Near-Field Dosimetry for In Vitro Exposure of Human Cells at 60 GHz

Maxim Zhadobov,[1]* Ronan Sauleau,[1] Robin Augustine,[1] Catherine Le Quément,[2] Yves Le Dréan,[2] and Daniel Thouroude[1]

[1]*Institute of Electronics and Telecommunications of Rennes (IETR), UMR CNRS 6164, University of Rennes 1, Rennes, France*
[2]*Intracellular Protein Homeostasis (HIP), IFR 140, UMR CNRS 6026, University of Rennes 1, Rennes, France*

Due to the expected mass deployment of millimeter-wave wireless technologies, thresholds of potential millimeter-wave-induced biological and health effects should be carefully assessed. The main purpose of this study is to propose, optimize, and characterize a near-field exposure configuration allowing illumination of cells in vitro at 60 GHz with power densities up to several tens of mW/cm^2. Positioning of a tissue culture plate containing cells has been optimized in the near-field of a standard horn antenna operating at 60 GHz. The optimal position corresponds to the maximal mean-to-peak specific absorption rate (SAR) ratio over the cell monolayer, allowing the achievement of power densities up to 50 mW/cm^2 at least. Three complementary parameters have been determined and analyzed for the exposed cells, namely the power density, SAR, and temperature dynamics. The incident power density and SAR have been computed using the finite-difference time-domain (FDTD) method. The temperature dynamics at different locations inside the culture medium are measured and analyzed for various power densities. Local SAR, determined based on the initial rate of temperature rise, is in a good agreement with the computed SAR (maximal difference of 5%). For the optimized exposure setup configuration, 73% of cells are located within the ±3 dB region with respect to the average SAR. It is shown that under the considered exposure conditions, the maximal power density, local SAR, and temperature increments equal 57 mW/cm^2, 1.4 kW/kg, and 6 °C, respectively, for the radiated power of 425 mW. Bioelectromagnetics 33:55–64, 2012.

Key words: dosimetry; millimeter waves; near-field exposure; optimization

INTRODUCTION

The rapid progress in integrated technologies at millimeter waves [Niknejad, 2010] and the increasing demand for higher data rate communications and mobility have triggered an exponential interest in the development of new millimeter-wave wireless applications [Xiao et al., 2008]. In particular, one of the objectives of the Wireless High Definition Interest Group (WiHD) and the Wireless Gigabit Alliance (WiGig) is to develop broadband short-range communication systems and promote new standards for indoor wireless high-definition multimedia transmissions at 60 GHz [WiHD, 2011; WiGig, 2011]. Compared to the already available wireless microwave technologies, the advantages of these upcoming systems are numerous, including faster data rates (over 2 Gbit/s), large and license-free bandwidth, reduced antenna size, and low interference between devices. Integrated front-ends at 60 GHz are expected to be commercialized by 2014 on laptops, and millimeter-wave body-centric communication systems are now under study.

According to the International Commission on Non-Ionizing Radiation Protection (ICNIRP) guidelines, commonly used as a reference for the safety exposure limits in the 60-GHz band [ICNIRP, 1998], the incident power density (IPD) averaged over 20 cm^2 is limited to 1 mW/cm^2 for the general public and 5 mW/cm^2 for workers. However, spatial maximum power densities up to 20 mW/cm^2 (general

Grant sponsors: Agence Nationale de la Recherche (ANR), France (Bio-CEM project); Grant number: ANR-09-RPDOC-003-01; Centre National de la Recherche Scientifique (CNRS), France.

*Correspondence to: Maxim Zhadobov, Institute of Electronics and Telecommunications of Rennes (IETR), University of Rennes 1, 11D, 263 av. du G. Leclerc, 35042 Rennes, France. E-mail: maxim.zhadobov@univ-rennes1.fr

Received for review 26 February 2011; Accepted 30 May 2011

DOI 10.1002/bem.20685
Published online 28 June 2011 in Wiley Online Library (wileyonlinelibrary.com).

public) and 100 mW/cm^2 (workers) are permitted for local exposure scenarios (power density averaged over 1 cm^2) [ICNIRP, 1998]. Exposures under these conditions have had a limited practical interest so far, but should now be studied in detail due to the expected development of body-centric communication systems [Xiao et al., 2008]. In such systems, antennas are placed directly on the body inducing localized exposures of the superficial body layers. In this context, it is fundamental to identify power density thresholds of potential biological consequences in order to precisely determine safe exposure limits.

In the past several years, biocompatibility issues related to near-future environmental millimeter-wave exposures have been investigated [Zhadobov et al., 2011]. As far as biological results are concerned, some scientific reports suggest that there are no significant reproducible changes due to the exposure to low-power electromagnetic fields below 1 mW/cm^2 at 60 GHz [Zhadobov et al., 2007, 2009; Nicolas et al., 2009a,b], whereas other recent publications demonstrated changes in cell membrane potential at μW/cm^2 levels [Pikov et al., 2010; Siegel and Pikov, 2010; Gapeyev et al., 2011].

In parallel, several studies have been conducted at medium-power levels (typically 1–10 mW/cm^2) on the potential biomedical applications of millimeter waves [Pakhomov et al., 1998; Radzievsky et al., 2008; Ramundo-Orlando et al., 2009]. In most of these works, cells, animals, or humans have been locally exposed by a horn antenna. In contrast to low-power exposures, these induce a superficial heating (typically 1–2 °C, depending on the antenna and exposure area [Alekseev et al., 2010]), which is partly compensated by the blood flow in in vivo models. The local exposure of the skin at millimeter waves has been extensively investigated from electromagnetic and thermodynamic points of view [Alekseev et al., 2008a,b; Alekseev and Ziskin, 2009a,b]. Moreover, several experimental techniques have been introduced to quantify thermal effects resulting from millimeter-wave exposure; they are summarized in Zhadobov et al. [2011]. In addition, some recent studies have demonstrated that high-power millimeter-wave exposures (160 mW/cm^2) may result in biological effects that are different from those observed for equivalent temperature increments induced by infrared heating [Alekseev et al., 2010].

In this context, the accurate electromagnetic and thermal analysis of the power-dependent thresholds and potential combined electromagnetic/thermal millimeter-wave induced effects at the cellular level is of utmost importance. This requires development of specific exposure systems [Paffi et al., 2010].

Free-space exposure set-ups or anechoic chambers have been previously used in most of the studies on cell or animal exposures to millimeter waves [Szabo et al., 2001, 2003; Safronova et al., 2002; Chen et al., 2004; Zhao and Wei, 2005; Siegel and Pikov, 2010]. Far-field set-ups allow simultaneous exposure of several samples and provide a nearly uniform distribution of the power density over a sample set (typical deviations of the power density are less than 30%) and a low peak-to-mean power density ratio. However, the efficiency of far-field exposure systems is low (less than 10–15%), which results in low power density levels in the biological samples (below several mW/cm^2). For a given radiating structure, there are two possible solutions to achieve higher power densities: increase the output power or bring the sample closer to the antenna. The first solution implies using high-power generators that are not always available for research purposes. The second one requires characterization of the near-field distribution in presence of biological samples in the reactive zone. For the implementation of the second approach, accurate dosimetry and optimization of the near-field exposure set-ups is crucial, as significant deviations of the temperature and specific absorption rate (SAR) profiles may appear even for small displacements (several millimeters) between an antenna and a sample.

In this study, we propose and optimize a near-field configuration of an exposure system at 60 GHz with high power densities (up to several tens of mW/cm^2) for in vitro experiments. In order to extensively characterize exposure levels, three complementary parameters have been determined and analyzed, namely the power density, SAR, and temperature dynamics.[1]

MATERIALS AND METHODS

Exposure Set-Up

In this study, cells were illuminated under near-field conditions by a standard 16.2-dBi-gain pyramidal horn antenna (Fig. 1) within a compact temperature-controlled anechoic exposure chamber. The main hardware parts of the experimental set-up, namely the narrowband 60-GHz power generator, frequency and power control unit, and exposure chamber, were previously reported for a far-field configuration [Zhadobov et al., 2009].

[1]Some preliminary numerical results have been presented at the European Conference on Antennas and Propagation (EuCAP), 2010 [Zhadobov et al., 2010].

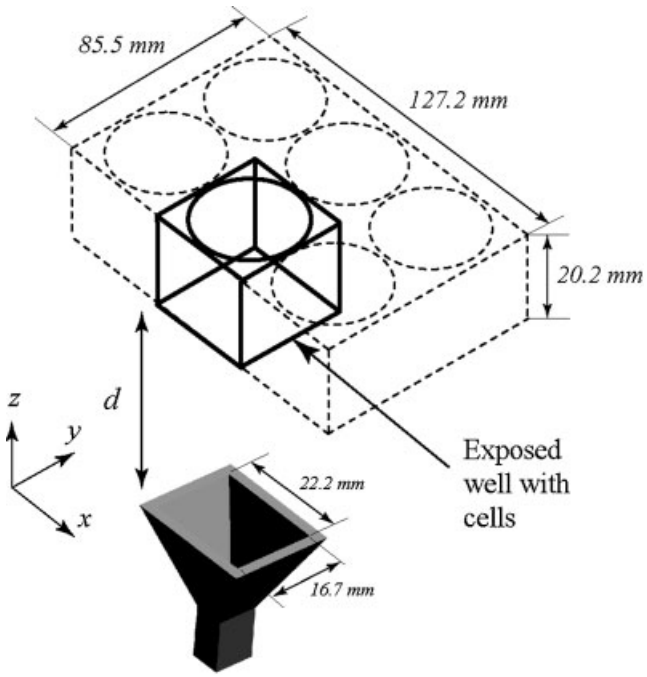

Fig. 1. 3D view of the pyramidal horn antenna and tissue culture plate. Solid lines: exposed well; dashed lines: empty wells.

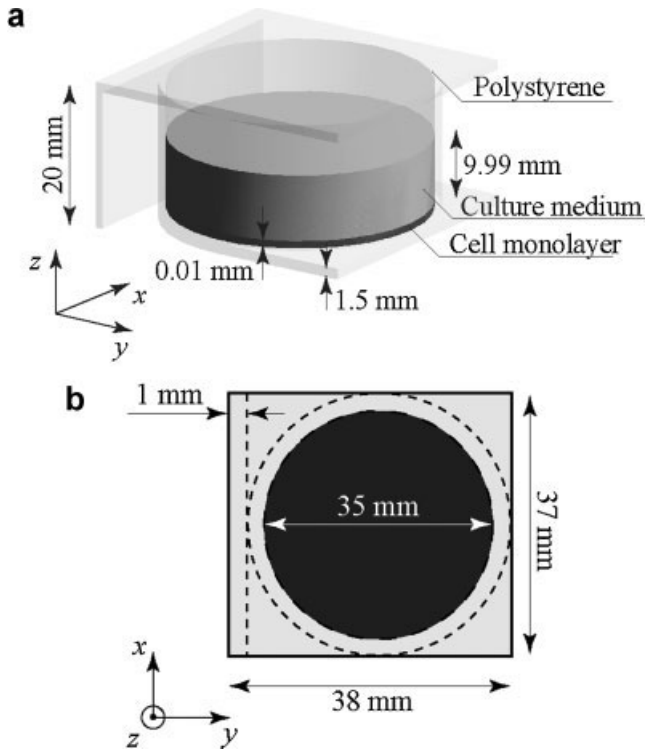

Fig. 2. Geometry of the exposed well containing the culture medium and cells. **a**: 3D view. **b**: Top view.

The 10-μm thick cell monolayer is located at the bottom of a central well (35 mm in diameter) of a standard 6-well tissue culture plate (8.6×12.7 cm^2) and is covered by a 1-cm thick tissue culture medium (Fig. 2). Human keratinocyte cells have been considered since they are the main constituents of the skin and, in case of whole-body exposures, are the primary target of millimeter waves. The antenna aperture dimensions, inner cross-section of the rectangular WR-15 feeding waveguide (V-band) operating in the TE_{10} fundamental wave mode, and axial distance from the waveguide/horn interface to the aperture equal 22.2×16.7 mm^2, 3.75×1.88 mm^2, and 18.9 mm, respectively. Computed return loss of the antenna was below -20 dB at 60 GHz for the antenna in free space, as well as for the antenna in front of the tissue culture plate.

The positioning (distance d in Fig. 1) of the exposed sample is optimized to extend the range of incident power densities at least up to 50 mW/cm^2 (for a fixed radiated power of 425 mW) and ensure high mean-to-peak SAR ratio within a cell layer (all other exposure arrangements being the same as in Zhadobov et al. [2009]). To this end, a parametric study has been carried out (refer to Optimization of the Exposure Set-Up Configuration Section). The results show that the optimal value of d equals 25 mm at 60 GHz.

Numerical Electromagnetic Model

The accurate measurement of the local power density and SAR with a spatial resolution better than 1 mm is a very challenging task for millimeter-wave exposures. Practically, the experimental dosimetry at these frequencies involves the use of relatively large probes (with dimensions on the order of one-half of the free-space wavelength). Moreover, these probes may significantly perturb the near-field distribution, which makes them inappropriate for near-field local measurements. Furthermore, indirect dosimetric techniques, for instance, infrared thermometry, are not appropriate in this experimental configuration since the cell monolayer is separated from the air by a lossy (at infrared frequencies) polystyrene layer. Therefore, we focused on the numerical analysis in this part of the study.

The geometric model used for numerical simulations is represented in Figures 1 and 2. Only the feed antenna and one well of the tissue culture plate (shown by solid lines in Fig. 1) have been simulated to reduce the total computational volume represented for each simulation by over 50 million mesh cells. As the dielectric permittivity and electrical conductivity of polystyrene at 60 GHz are much smaller than those of cells and culture media [Zhadobov

et al., 2008], the contribution of the reflections from the neighboring empty wells to the SAR distribution is expected to be negligible. The meniscus effect, considered an important factor for frequencies around 1 GHz, is neglected since the skin depth of the 60-GHz radiation is much smaller than the thickness of the culture medium.

The dielectric properties of the well and biological samples at 60 GHz are given in Table 1. The complex permittivity of the cells has been determined as explained by Zhadobov et al. [2008]. The complex permittivity of the culture medium has been measured at 37 °C using a slim open-ended coaxial probe provided by Agilent (Oberhaching, Germany).

The finite-difference time-domain (FDTD) method has been used to conduct this numerical dosimetry study. Small substructures including the cell monolayer have been carefully taken into account using non-uniform adaptive meshing. The electromagnetic simulations have been carried out using the conformal FDTD solver SEMCAD X provided by Schmid & Partner (Zurich, Switzerland). All simulations have been performed using a FDTD mesh with a cell size ranging from $\lambda_c/137 = 0.005$ mm (in the cell layer in z direction) up to $\lambda_0/20 = 0.25$ mm (in free space), where $\lambda_c = 0.685$ mm and $\lambda_0 = 5$ mm are the wavelength in the cell monolayer and the free-space wavelength, respectively. Mesh cell size in x and y directions ranges from 0.05 to 0.25 mm. The numerical results have also been confirmed using an XFDTD solver (REMCOM, State College, PA). In the simulations, we assume that the dielectric permittivity, conductivity, and mass density are temperature independent in the 37–43 °C temperature range.

Thermal Measurements

Temperature increase should be carefully characterized for medium- and high-power exposures of living systems to millimeter waves as temperature increments can lead to biological consequences for both in vitro and in vivo models. Here, we experimentally analyze the transient heating and steady-state thermal dynamics within the biosamples exposed at 60 GHz.

TABLE 1. Dielectric Properties Used for the Numerical Modeling at 60 GHz

Substructure/material	Relative permittivity	Conductivity (S/m)
Background/air	1	0
Antenna/perfect electric conductor	—	∞
Tissue culture plate/polystyrene	2.3	0.001
Culture medium	15.5	83.8
Cells	10.9	50.4

The measurements have been performed using a 4-channel Reflex fiber optic thermometer (NEOPTIX, Québec, Canada) as shown in Figure 3. The fiber can be fixed in nine different positions using a specific holder made of Teflon, attached to the upper side of the well cover. The temperature is recorded at the tip of the fiber (0.4 mm in diameter) with 0.01 °C resolution and relative accuracy of ±0.05 °C. Absolute accuracy of measurements was adjusted at 37 °C with ±0.1 °C precision using a water etalon with known temperature.

RESULTS

Optimization of the Exposure Set-Up Configuration

The purpose of the optimization of the positioning of the tissue culture plate is to find the optimal relationship between the peak-to-mean SAR over the cell monolayer (to be minimized) and IPD (to be maximized). The strategy implemented for optimization consists of two parts.

First, the maximum power density (PD_{max}) and the power density averaged over the surface corresponding to the cell monolayer area (PD_{av}) are computed in free space in several horizontal planes parallel to the antenna aperture and located at different distances (d) from the antenna (from 0 to 70 mm). The cost function ($F_{PD}(d)$) used to optimize the distance d is defined as follows:

$$F_{PD}(d) = \left(\frac{PD_{av}}{PD_{max}}\right) PD_{av} \quad (1)$$

The factor PD_{av}/PD_{max} represents the mean-to-peak power density ratio; it increases with d, whereas the second factor, PD_{av}, decreases as a function of d. Figure 4 shows F_{PD} as a function of d. Three distances (20, 25, and 30 mm) corresponding to values of F_{PD} close to its maximum are chosen for further optimization because this methodology does not guarantee the optimal SAR distribution within the cell layer.

Second, using the three preselected distances, the optimal value of d is determined based on the SAR distribution within the cell layer. The cost function to be maximized is similar to the one used in Equation (1):

$$F_{SAR}(d) = \left(\frac{SAR_{av}}{SAR_{max}}\right) SAR_{av} \quad (2)$$

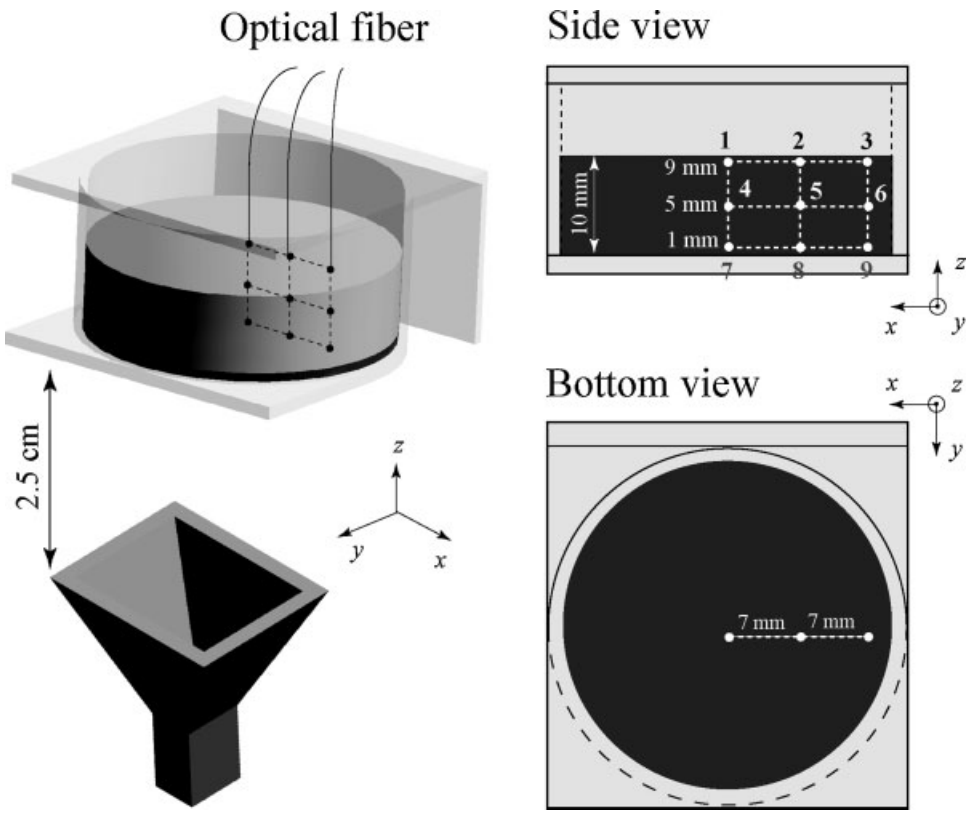

Fig. 3. Schematic representation of the temperature measurement set-up. The temperature is monitored within the culture medium using a fiber optic thermometer. White dots (side view) refer to the locations of the fiber tip. Dimensions of the well are given in Figure 2.

where SAR_{av} and SAR_{max} are the average and maximum SAR values within the cell layer, respectively. The values of $F_{SAR}(d)$, as well as SAR_{av} and SAR_{max} for $d = 20$, 25, and 30 mm are summarized in Table 2. According to these results, the optimum distance d is 25 mm.

For this configuration, three major dosimetry characteristics have been considered in detail: (1) the power density—the main dosimetric quantity in the 10–300 GHz range; (2) the SAR, which also takes into account the dielectric (conductivity) and physical (mass density) properties of the exposed samples; and (3) the temperature distribution and dynamics, particularly important for medium- or high-power exposures.

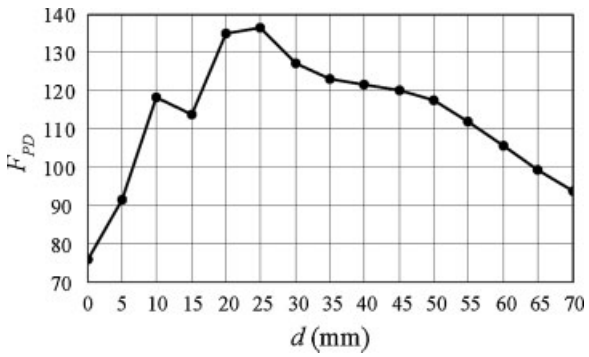

Fig. 4. Cost function used to optimize the distance between the antenna and tissue culture plate.

Electromagnetic Dosimetry

The IPD, as well as the local and average SAR and the power loss within the cell monolayer have been computed and analyzed. The maximum radiated power of the horn antenna is 425 mW at 60 GHz (this corresponds to the maximum radiated power

TABLE 2. SAR-Based Optimization of the Distance Between the Antenna and Tissue Culture Plate

d (mm)	$F_{SAR}(d)$	SAR_{av} (W/kg)	SAR_{max} (W/kg)
20	210	720	2471
25	325	673	1393
30	183	506	1397

that can be delivered by our millimeter-wave source [Zhadobov et al., 2009]).

Local SAR distributions within the cell monolayer computed at 60 GHz are represented in Figure 5a in the horizontal cross-section, and in Figure 5b,c in several vertical cut-planes. The results demonstrated that 73% of the cells are located within the ±3 dB region, relative to the average SAR value; and 83% of cells are located within the ±5 dB region. The computed standard deviation of the local SAR within the cell layer equals 383.3 W/kg (±28%) compared to the average SAR within the cell monolayer. The computed total power loss within the cell layer and within the culture medium equals 7 and 180 mW, respectively.

In order to estimate the variability of the considered characteristics as a function of frequency, we computed the IPD and maximum, minimum, and average SAR at eight discrete frequencies within the 57–64 GHz range for the radiated power of 425 mW. The antenna/tissue culture plate separation d was the same as for the 60-GHz configuration (25 mm). The data, mean value for each parameter over the considered frequency range, and standard deviation are summarized in Table 3. These results demonstrate that a 1 GHz shift significantly changes the SAR and IPD values. This demonstrates that the frequency stability, as well as positioning of the tissue culture plate should be precisely controlled during the exposure experiments in order to ensure the reproducibility.

As the power density and SAR increase linearly with the radiated power, the following relationship can be derived for the considered characteristics based on the data obtained at 60 GHz:

$$\begin{aligned} \mathrm{SAR_{max}[W/kg]} &= 30 \times \mathrm{SAR_{min}[W/kg]} \\ &= 2 \times \mathrm{SAR_{av}[W/kg]} \\ &= 25.3 \times \mathrm{IPD[mW/cm^2]} = 3.3 \times P_0\mathrm{[mW]} \end{aligned} \quad (3)$$

The maximum IPD value that can be extracted from this exposure set-up at 60 GHz is 57 mW/cm^2. This satisfies the requirements defined in Exposure Set-up Section.

Measurements of the Temperature Dynamics

From the numerical modeling point of view, the determination of the temperature dynamics within biological samples exposed to millimeter waves is a difficult task as many parameters should be carefully taken into account. These include: (1) the SAR induced in the cell layer and culture medium

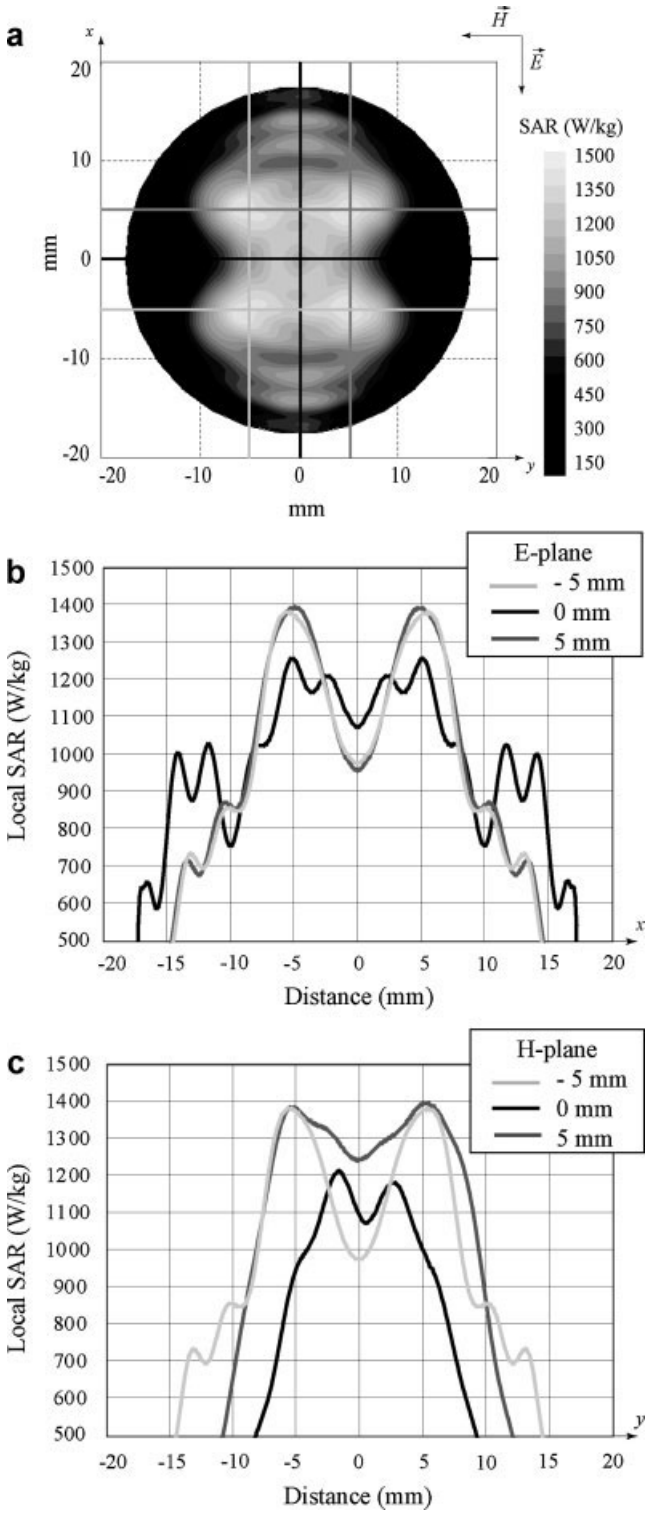

Fig. 5. Computed distribution of the local SAR within the cell monolayer exposed at 60 GHz for a radiated power of 425 mW. **a**: Local SAR at the half-height of the cell monolayer (5 μm). **b**: Vertical profiles in E-plane. **c**: Vertical profiles in H-plane. These profiles correspond to the six cut planes shown in (a).

TABLE 3. SAR and IPD at Eight Discrete Frequencies Within the 57–64 GHz Range (Radiated Power Is 425 mW)

f (GHz)	SAR_{max} (W/kg)	SAR_{min} (W/kg)	SAR_{av} (W/kg)	IPD (mW/cm^2)
57	1960	95	582	60
58	2315	37	673	91
59	1830	8	558	70
60	1397	46	673	57
61	1877	76	793	60
62	1605	6	573	53
63	1522	55	572	55
64	3530	31	832	111
57–64 (mean/SD)	2005/680	44/31	657/106	70/21

considered as a thermal source; (2) thermal properties of the cells and culture medium and boundary conditions that must be properly defined; and (3) thermal conductivity, convection, and radiation phenomena. Furthermore, thermoregulation within the incubator during exposure should also be taken into account. As a consequence, the numerical results for the temperature distributions could significantly deviate from real values.

An alternative solution is to measure the temperature dynamics. To this end, we used a fiber optic thermometer. In addition to the compact size and possibility to locally monitor the temperature dynamics, the fiber optic probe does not perturb the electromagnetic field distribution within the sample.

Figure 6 represents the temperature dynamics within the well exposed at 60 GHz for a radiated power of 425 mW. The temperature profiles are shown for the different locations of the fiber tip (Fig. 3). The fiber tip was immersed in the culture medium, and the exposure started after a stabilization period of 5 h. The exposure was launched (time point $t = 0$) only if the temperature stability for the last 2 h was better than ± 0.1 °C. The maximal and minimal measured temperature increments equal 6.1 and 4 °C, respectively.

These results have been compared to the temperature data obtained for distilled water (Fig. 7). Figures 6 and 7 show that the temperature dynamics are roughly the same in both cases (the maximal temperature difference is only $\pm 3\%$), suggesting that the dielectric and thermodynamic properties of water and culture medium are close.

A temperature-based SAR determination method was used for the cross comparison of numerical and experimental results for distilled water. Experimentally, the average near-surface SAR was determined using the data for the initial rate of temperature rise in points 7, 8, and 9 (Fig. 3)

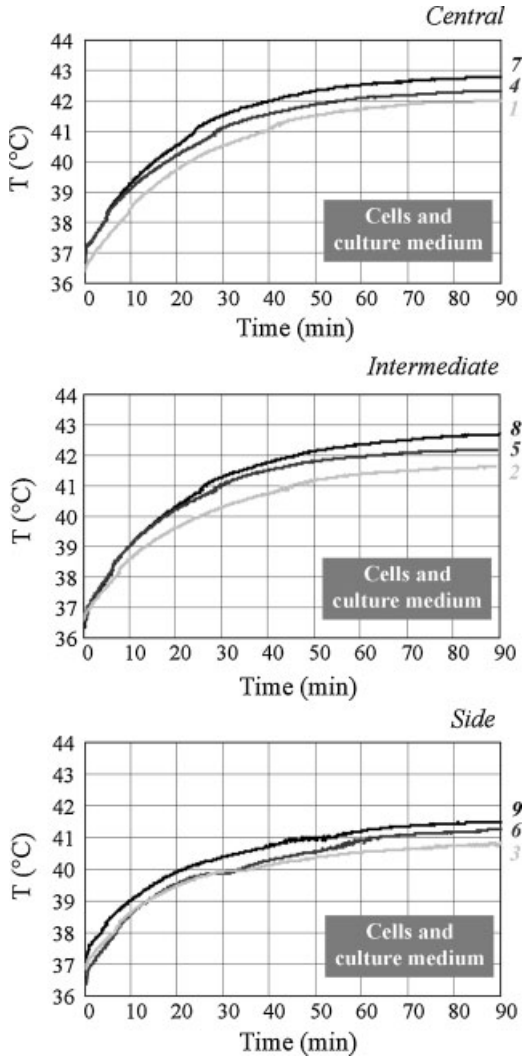

Fig. 6. Temperature dynamics measured in nine locations within the well containing the cells and culture medium. Numbers on the right of the graphs correspond to the locations of the fiber optic probe as shown in Figure 3.

according to the formula:

$$\mathrm{SAR} = C\left.\frac{\mathrm{d}T}{\mathrm{d}t}\right|_{t=0} \tag{4}$$

The initial rise rate of the near-surface temperature was determined by fitting the experimental heating dynamics for the first 30 s of exposure to a theoretical thermal model issued from the 1D heat transfer equation [Walters et al., 2000]. The SAR was calculated using the specific heat capacity $C = 4200$ J/kg °C (Table 4). Numerical and experimental results are in a good agreement (maximal deviation of 5%).

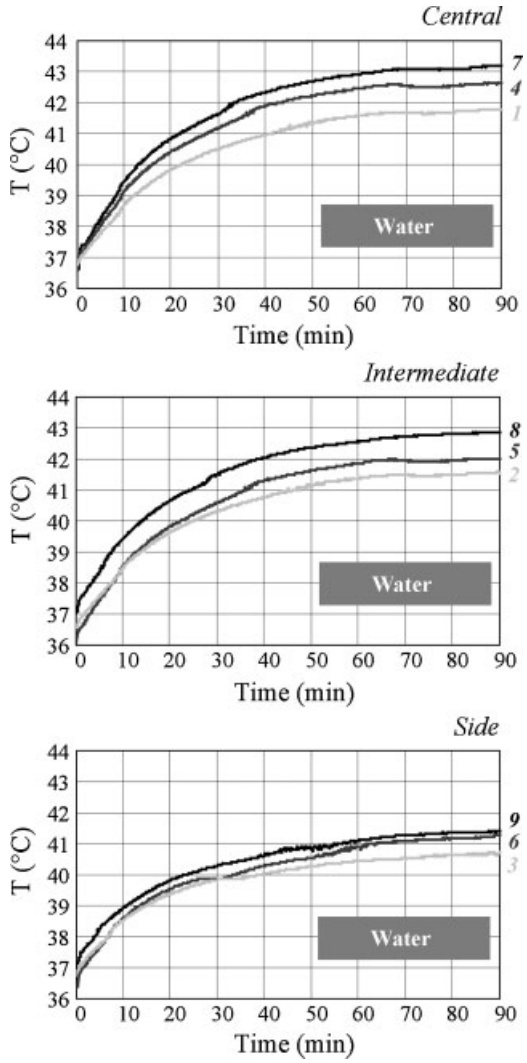

Fig. 7. Temperature dynamics measured in nine locations within the well containing distilled water. Numbers on the right of the graphs correspond to the locations of the fiber optic probe as shown in Figure 3.

Figure 8a represents the temperature dynamics measured within the well containing cells and culture medium for several values of the radiated power. The temperature is monitored at point 7 (Fig. 3). The results shown in Figure 8b suggest a quasi-linear

TABLE 4. Cross Comparison of Computed and Experimentally Determined Local SAR

	Observation point		
SAR (W/kg)	7	8	9
Computations	1693	1647	1583
Temperature measurements	1604	1571	1551
Relative deviation	5.3%	4.6%	2%

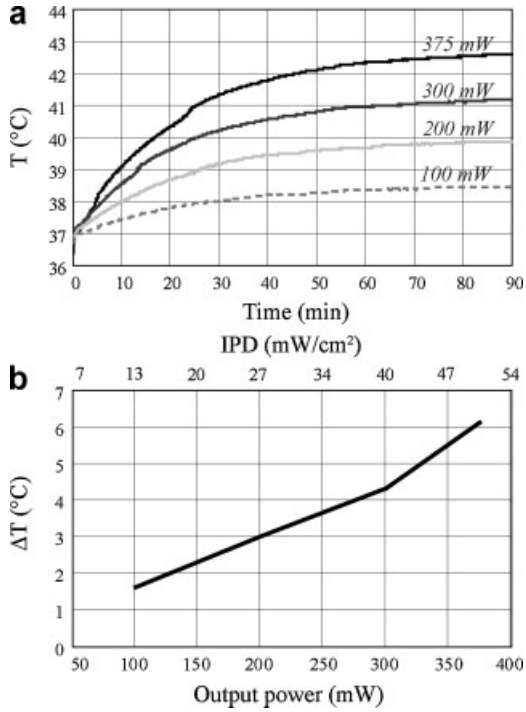

Fig. 8. **a**: Temperature dynamics for several values of the radiated power. **b**: Measured peak temperature increment as a function of the radiated power and IPD.

behavior of the steady-state temperature increments as a function of the radiated power within the considered power range that can be expressed as:

$$\Delta T(^\circ C) = 8.1 \times \mathrm{IPD(mW/cm^2)} = 60.5 \times P_0(\mathrm{mW}) \quad (5)$$

The presented results take into account convection resulting in the cooling of the lower part of the culture medium during the exposure, and heating of the upper part.

It is worthwhile to recall that the experiments have been carried out in a thermo-controlled incubator representative of the experimental conditions of in vitro exposures. Practically, if the temperature increments are known, the initial temperature of the incubator could be decreased by the value of the corresponding temperature increment in order to avoid any heat shock in the cells.

CONCLUSION

A near-field configuration of a 60-GHz exposure system for in vitro studies has been proposed, and the positioning of the tissue culture plate relative to the antenna was optimized to maximize the mean-

to-peak SAR ratio while achieving incident power densities up to several tens of mW/cm^2.

An in-depth numerical dosimetry analysis has been performed for the selected configuration in order to accurately characterize the power density and SAR. It was shown that incident power densities up to 57 mW/cm^2 are achievable at 60 GHz for the radiated power of 425 mW. The local SAR distributions within the cell monolayer and average SAR as a function of the power density have been computed. The results demonstrate that 73% of cells are located within the $\pm$3 dB region with respect to the average SAR. The maximal and averaged SAR over the cell monolayer is equal to 1.4 kW/kg and 673 W/kg, respectively. Results obtained for eight discrete frequencies within the 57–64 GHz range demonstrated the maximal difference of the average SAR within the cell monolayer is 31% for a 1 GHz frequency shift; however, the maximal deviation is 17% for the 59–61 GHz range.

The temperature dynamics as a function of the radiated power have been measured and analyzed at nine points within the exposed well. It is shown that under the considered exposure conditions, temperature elevations up to 2.3 and 6 °C can be reached for 20 and 50 mW/cm^2, respectively. Local SAR, determined based on the initial rate of temperature rise, was in good agreement with the computed SAR (difference less than 5%), confirming the reliability of numerical and experimental results.

ACKNOWLEDGMENTS

The authors acknowledge Peter Futter from Schmid & Partner Engineering AG, Zurich, Switzerland, for the technical support in numerical simulations.

REFERENCES

Alekseev SI, Gordiienko OV, Ziskin MC. 2008a. Reflection and penetration depth of millimeter waves in murine skin. Bioelectromagnetics 29(5):340–344.

Alekseev SI, Radzievsky AA, Logani MK, Ziskin MC. 2008b. Millimeter-wave dosimetry of human skin. Bioelectromagnetics 29(1):65–70.

Alekseev SI, Ziskin MC. 2009a. Influence of blood flow and millimeter wave exposure on skin temperature in different thermal models. Bioelectromagnetics 30(1):52–58.

Alekseev SI, Ziskin MC. 2009b. Millimeter-wave absorption by cutaneous blood vessels: A computational study. IEEE Trans Biomed Eng 56(10):2380–2388.

Alekseev SI, Gordiienko OV, Radzievsky AA, Ziskin MC. 2010. Millimeter-wave effects on electrical responses of the sural nerve in vivo. Bioelectromagnetics 31(3):180–190.

Chen Q, Zeng Q, Lu D, Chiang H. 2004. Millimeter wave exposure reverses TPA suppression of gap junction intercellular communications in HaCaT human keratinocytes. Bioelectromagnetics 25:2–4.

Gapeyev AB, Kulagina TP, Aripovsky AV, Chemeris NK. 2011. The role of fatty acids in anti-inflammatory effects of low-intensity extremely high-frequency electromagnetic radiation. Bioelectromagnetics 32:388–395.

ICNIRP. 1998. Guidelines for limiting exposure to time-varying electric, magnetic, and electromagnetic fields (up to 300 GHz). Health Phys 74(4):494–522.

Nicolas Nicolaz C, Zhadobov M, Desmots F, Ansart A, Sauleau R, Thouroude D, Michel D, Le Dréan Y. 2009a. Study of narrow band millimeter-wave potential interactions with endoplasmic reticulum stress sensor genes. Bioelectromagnetics 30:365–373.

Nicolas Nicolaz C, Zhadobov M, Desmots F, Sauleau R, Thouroude D, Michel D, Le Dréan Y. 2009b. Absence of direct effect of low-power millimeter-wave radiation at 60.4 GHz on endoplasmic reticulum stress. Cell Biol Toxicol 25(5):471–478.

Niknejad AM. 2010. Siliconization of 60 GHz. IEEE Microwave Mag 11(1):78–85.

Paffi A, Apollonio F, Lovisolo GA, Marino C, Pinto R, Repacholi M, Liberti M. 2010. Considerations for developing an RF exposure system: A review for in vitro biological experiments. IEEE Trans Microwave Theory Tech 58(10):2702–2714.

Pakhomov AG, Akyel Y, Pakhomova ON, Stuck BE, Murphy MR. 1998. Current state and implications of research on biological effects of millimeter waves: A review of the literature. Bioelectromagnetics 19(7):393–413.

Pikov V, Arakaki X, Harrington M, Fraser SE, Siegel P. 2010. Modulation of neuronal activity and plasma membrane properties with low-power millimeter waves in organotypic cortical slices. J Neural Eng 7(4):045003.

Radzievsky AA, Gordiienko OV, Alekseev SI, Szabo I, Cowan A, Ziskin MC. 2008. Electromagnetic millimeter wave induced hypoalgesia: Frequency dependence and involvement of endogenous opioids. Bioelectromagnetics 29(4): 284–295.

Ramundo-Orlando A, Longo G, Cappelli M, Girasole M, Tarricone L, Beneduci A, Massa R. 2009. The response of giant phospholipid vesicles to millimeter waves radiation. Biochim Biophys Acta 1788:1497–1507.

Safronova VG, Gabdoulkhakova AG, Santalov BF. 2002. Immunomodulating action of low intensity millimeter waves on primed neutrophils. Bioelectromagnetics 23: 599–606.

Siegel P, Pikov V. 2010. Impact of low intensity millimetre waves on cell functions. Electron Lett 46(26):70–72.

Szabo I, Rojavin MA, Rojers TJ, Ziskin MC. 2001. Reaction of keratinosytes to in vitro millimeter wave exposure. Bioelectromagnetics 22:358–364.

Szabo I, Manning MR, Radzievsky AA, Wetzel MA, Rojers TJ, Ziskin MC. 2003. Low power millimeter wave irradiation exerts no harmful effect on human keratinocytes in vitro. Bioelectromagnetics 24:65–173.

Walters TJ, Blick DW, Johnson LR, Adair ER, Foster KR. 2000. Heating and pain sensation produced in human skin by millimeter waves: Comparison to a simple thermal model. Health Phys 78(3):259–267.

WiGig (Wireless Gigabit Alliance). 2011. http://wirelessgigabitalliance.org (Last accessed 15 February 2011).

WiHD (Wireless High Definition). 2011. www.wirelesshd.org (Last accessed 15 February 2011).

Xiao S-Q, Zhou M-T, Zhang Y. 2008. Millimeter wave technology in wireless PAN, LAN, and MAN. Boca Raton, FL: CRC Press.

Zhadobov M, Sauleau R, Le Coq L, Debure L, Thouroude D, Michel D, Le Dréan Y. 2007. Low-power millimeter wave radiations do not alter stress-sensitive gene expression of chaperone proteins. Bioelectromagnetics 28:188–196.

Zhadobov M, Sauleau R, Le Dréan Y, Alekseev SI, Ziskin MC. 2008. Numerical and experimental millimeter-wave dosimetry for in vitro experiments. IEEE Trans Microwave Theory Tech 56(12):2998–3007.

Zhadobov M, Nicolas Nicolaz C, Sauleau R, Desmots F, Thouroude D, Michel D, Le Dréan Y. 2009. Evaluation of the potential biological effects of the 60-GHz millimeter waves upon human cells. IEEE Trans Antennas Propag 57(10):2949–2956.

Zhadobov M, Sauleau R, Thouroude D, Nicolas Nicolaz Ch, Le Quement C, Le Drean Y. 2010. Near-field electromagnetic dosimetry for in vitro studies at millimeter waves. Barcelona, Spain: EuCAP. pp 1–3.

Zhadobov M, Chahat N, Sauleau R, Le Quément C, Le Dréan Y. 2011. Millimeter-wave interactions with the human body: State of knowledge and recent advances. Int J Microwave Wireless Technol 3(2):237–247.

Zhao JX, Wei Z. 2005. Numerical modeling and dosimetry of the 35 mm Petri dish under 46 GHz millimeter wave exposure. Bioelectromagnetics 26:481–488.